CREEP BUCKLING BEHAVIOR OF HIGH-STRENGTH CONCRETE PANELS IN TWO-WAY ACTION

Yue Huang[1,*], Ehab Hamed[1], Stephen Foster[1]
[1]Centre for Infrastructure Engineering and Safety, School of Civil and Environmental Engineering,
The University of New South Wales, Sydney, NSW 2052, Australia. *Email: yue.huang2@unsw.edu.au

ABSTRACT

The nonlinear long-term behavior of slender high-strength concrete (HSC) panels in two-way action is investigated in this paper. A theoretical model that considers the geometric nonlinearity and creep of concrete is developed based on a time-stepping analysis. A rheological material model that is based on the generalized Maxwell chain is adopted to model the concrete creep. Von Karman plate theory is used to derive the incremental governing equations. The equations are solved numerically at each time step based on a Fourier series expansion of the deformations and loads in one direction, and using the numerical multiple shooting method in the other direction. The capabilities of the model are demonstrated through a numerical example and a parametric study. The numerical study shows that the model can effectively predict the time-dependent behavior of two-way HSC panels, where the out-of-plane deflection and internal bending moments increase with time as a result of the combined effects of creep and geometric nonlinearity. These effects may ultimately lead to creep buckling failures. A parametric study is carried out to investigate the effects of in-plane load level, load eccentricity and slenderness ratio. It is revealed that the long-term behavior of two-way HSC panels is very sensitive to these parameters.

KEYWORDS

Buckling, creep, panel, high strength concrete, time-dependent.

INTRODUCTION

High-strength concrete panels in two-way action have attracted numerous research interests in the past decades. Slender two-way concrete panel may undergo increasing in-plane and out-of-plane deformations with time under eccentric sustained in-plane and/or out-of-plane loads due to the combined effects of geometric nonlinearity and creep of concrete. This may cause excessive deflection and cracking when the structure is in serviceable state or may eventually lead to creep buckling failure of the panel.

Studies that focus on the buckling failure behavior of two-way panels under the influence of creep and shrinkage, regardless of normal-strength concrete (NSC) or HSC panels, cannot be found in the open literature. However, a significant amount of studies have been undertaken to investigate the nonlinear behavior of two-way reinforced concrete (RC) panels under short-term loads, in which many of them focus on NSC wall panels. Swartz et al. (1974) tested 24 NSC panels that were subjected to uniaxial compressive loads along their short edges and simply supported along all four edges. The panels in the test failed due to buckling where the compressive stress levels varied from 51% to 87% of the concrete compressive strength. The paper also presented a formula, which was explained in details in Swartz and Rosebraugh (1974), for predicting the buckling load of RC panels. Saheb and Desayi (1990) tested 24 rectangular reinforced NSC wall panels loaded eccentrically in two-way action and simply-supported along four edges. It was found that the ultimate strength of wall panels in two-way action increased linearly with the increase of the aspect ratio as well as the vertical reinforcement. On the other hand, it reduced nonlinearly with the increase in thinness or slenderness ratios. Aghayere and Macgregor (1990a) reported test results on 9 concrete plates, simply supported along four edges and subjected to combined uniform in-plane compression and uniform transverse loading. Based on the test results, it can be concluded that in most axially loaded specimens, buckling of the reinforcement adjacent to the compression face took place at failure and all final failures were compression failures due to crushing of the concrete. Ghoneim and MacGregor (1994a) tested 19 two-way RC plates that were subjected to combined in-plane compressive and transverse loads. The test results indicated that the slenderness of the plate and the loading sequence mainly determined the effect of the in-plane load on the lateral load capacity of RC plates. Both material failure including crushing of concrete and yielding of the tension steel and stability failure occurred in the RC plates tested under combined

loads. Sanjayan and Maheswaran (1999) carried out experiments on 8 HSC concrete walls loaded eccentrically. It was found that the load capacity of the wall was significantly influenced by the eccentricity of in-plane loading, while it was insensitive to the concrete strength.

A number of theoretical analyses have also been carried out to study the behavior of two-way HSC panels (Aghayere and MacGregor 1990b; Massicotte et al. 1990; Ghoneim and MacGregor 1994b; Attard et al. 1996). Yet, their emphasis was placed on the short-term response where creep was not accounted for in the models.

Theoretical and experimental studies were conducted by Huang and Hamed (2013) and Huang (2015) to examine the time-dependent response of HSC panels in one-way actions. In this paper, a new theoretical model that utilizes the mechanics of thin plates is developed for the long-term analysis of HSC panels. A time-stepping analysis is used to account for the effect of creep. A rheological material model is adopted, which is based on the generalized Maxwell chain. In order to highlight the effect of creep only, a linear viscoelastic material behavior is assumed for concrete. The incremental governing equations are solved numerically at each time step based on a Fourier series expansion of the deformations and loads in one direction, and using the numerical multiple shooting method in the other direction. The mathematical formation of the model is presented first, followed by numerical and parametric studies.

MATHEMATICAL FORMULATION

The general governing equations derived here are applicable to any combination of external loads and boundary conditions. An incremental time-stepping analysis is implemented in order to account for the time-dependent change of the internal stresses and the increase of the deformations of the structure with time due to creep. For this, the time of concern t, which is measured from the time of first loading, is subdivided into n_t discrete time steps with $\Delta t_r = t_r - t_{r-1}$ ($r = 1, 2, \ldots, n_t$). The sign conventions for the coordinates, loads and displacements are shown in Figure 1. The middle plane of the panel is taken as the xy plane, where the x and y axes are directed along the edges. The z axis is taken normal to the middle plane and measured positive downwards. The forces and bending moments at the boundaries as well as the lateral loads are also presented in Figure 1. The torsional moments at the boundaries are not shown in the figure for brevity and clarity.

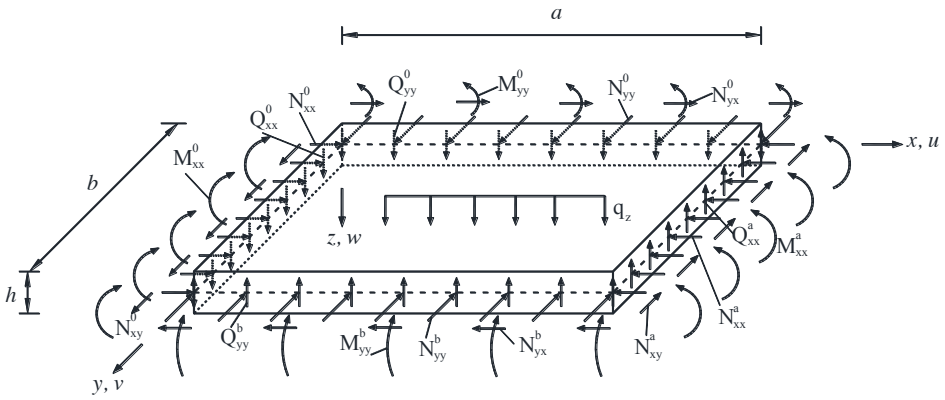

Figure 1 Sign conventions of the investigated panel

Kinematic Relations

In typical HSC panels, the dimensions in the z direction are much smaller than those in the other two directions. Therefore, a plane stress condition is adopted, where the stresses in the z direction including the normal and shear stresses are equal to zero. The theoretical model is based on Von Karman plate with large displacements. The incremental kinematic relations of the plate read

$$\Delta\varepsilon_{xx}(t_r) = \frac{\partial \Delta u(t_r)}{\partial x} + \frac{1}{2}\left(\frac{\partial \Delta w(t_r)}{\partial x}\right)^2 + \frac{\partial w(t_{r-1})}{\partial x}\frac{\partial \Delta w(t_r)}{\partial x} - z\frac{\partial^2 \Delta w(t_r)}{\partial x^2}$$

$$\Delta\varepsilon_{yy}(t_r) = \frac{\partial \Delta v(t_r)}{\partial y} + \frac{1}{2}\left(\frac{\partial \Delta w(t_r)}{\partial y}\right)^2 + \frac{\partial w(t_{r-1})}{\partial y}\frac{\partial \Delta w(t_r)}{\partial y} - z\frac{\partial^2 \Delta w(t_r)}{\partial y^2} \quad (1)$$

$$\Delta\gamma_{xy} = \frac{\partial \Delta u(t_r)}{\partial y} + \frac{\partial \Delta v(t_r)}{\partial x} - 2z\frac{\partial^2 \Delta w(t_r)}{\partial x \partial y} + \frac{\partial w(t_{r-1})}{\partial y}\frac{\partial \Delta w(t_r)}{\partial x} + \frac{\partial w(t_{r-1})}{\partial x}\frac{\partial \Delta w(t_r)}{\partial y} + \frac{\partial \Delta w(t_r)}{\partial x}\frac{\partial \Delta w(t_r)}{\partial y}$$

where ε_{xx} and ε_{yy} are the total normal strains in the x and y directions; γ_{xy} is the total shear strain in the xy planes. Each total strain has two components: the instantaneous strain and creep strain. u and v are the in-plane displacements along x and y directions, and w is the out-of-plane deflection along z axis, and $\partial/\partial x$ and $\partial/\partial y$ denote the partial derivative with respect to x and y, respectively; Δ represents the incremental operator and note that any displacement that appear without the Δ operator are the accumulated known quantity from the previous time step.

Equilibrium Equations

The variational principle of virtual work is used to derive the nonlinear incremental equilibrium equations along with the boundary conditions, where

$$\delta U + \delta W = 0 \tag{2}$$

with δU and δW as the internal virtual work and external virtual work and δ is the variational operator. The incremental equilibrium equations read

$$\frac{\partial \Delta N_{xx}}{\partial x} + \frac{\partial \Delta N_{xy}}{\partial y} = 0; \qquad \frac{\partial \Delta N_{yy}}{\partial y} + \frac{\partial \Delta N_{xy}}{\partial x} = 0 \tag{3}$$

$$\begin{aligned} &N_{xx}\frac{\partial^2 \Delta w}{\partial x^2} + \Delta N_{xx}\frac{\partial^2 w}{\partial x^2} + \Delta N_{xx}\frac{\partial^2 \Delta w}{\partial x^2} + N_{yy}\frac{\partial^2 \Delta w}{\partial y^2} + \Delta N_{yy}\frac{\partial^2 w}{\partial y^2} + \Delta N_{yy}\frac{\partial^2 \Delta w}{\partial x^2} \\ &+2N_{xy}\frac{\partial^2 \Delta w}{\partial x \partial y} + 2\Delta N_{xy}\frac{\partial^2 w}{\partial x \partial y} + 2\Delta N_{xy}\frac{\partial^2 \Delta w}{\partial x \partial y} + \frac{\partial^2 \Delta M_{xx}}{\partial x^2} + \frac{\partial^2 \Delta M_{yy}}{\partial y^2} + 2\frac{\partial^2 \Delta M_{xy}}{\partial x \partial y} + q_z = 0 \end{aligned} \tag{4}$$

where N_{xx} and N_{yy} are the internal axial forces in the x and y directions and N_{xy} are the internal shear force in the xy plane; M_{xx} and M_{yy} are the internal bending moments along x and y axes and M_{xy} is the internal torsional bending moment; q_z is the out-of-plane distributed load applied perpendicular to the top surface of the panel throughout the whole area. The general boundary conditions at $x = 0$ and $x = a$ are given by

$$\Delta N_{xx} + \Delta N^i_{xx} = 0 \quad \text{or} \quad \Delta u = \Delta \bar{u}; \qquad \Delta N_{xy} + \Delta N^i_{xy} = 0 \quad \text{or} \quad \Delta v = \Delta \bar{v}; \qquad \Delta M_{xx} - \Delta M^i_{xx} = 0 \quad \text{or} \quad \frac{\partial \Delta w}{\partial x} = \frac{\partial \Delta \bar{w}}{\partial x}$$

$$\begin{aligned} &N_{xx}\frac{\partial \Delta w}{\partial x} + \Delta N_{xx}\frac{\partial w}{\partial x} + \Delta N_{xx}\frac{\partial \Delta w}{\partial x} + N_{xy}\frac{\partial \Delta w}{\partial y} + \\ &\Delta N_{xy}\frac{\partial w}{\partial y} + \Delta N_{xy}\frac{\partial \Delta w}{\partial y} + \frac{\partial \Delta M_{xx}}{\partial x} + 2\frac{\partial \Delta M_{xy}}{\partial y} + \Delta Q^i_{xx} = 0 \qquad \text{or} \qquad \Delta w = \Delta \bar{w} \end{aligned} \tag{5}$$

where $\bar{u}$, $\bar{v}$, and $\bar{w}$ are the external deformations at the edges; and $i = 0$ at $x = 0$ and $i = a$ at $x = a$. The general boundary conditions at $y = 0$ and $y = b$ are given by

$$\Delta N_{yy} + \Delta N^i_{yy} = 0 \quad \text{or} \quad \Delta v = \Delta \bar{v}; \qquad \Delta N_{xy} + \Delta N^i_{yx} = 0 \quad \text{or} \quad \Delta u = \Delta \bar{u}; \qquad \Delta M_{yy} - \Delta M^i_{yy} = 0 \quad \text{or} \quad \frac{\partial \Delta w}{\partial x} = \frac{\partial \Delta \bar{w}}{\partial x}$$

$$\begin{aligned} &N_{yy}\frac{\partial \Delta w}{\partial y} + \Delta N_{yy}\frac{\partial w}{\partial y} + \Delta N_{yy}\frac{\partial \Delta w}{\partial y} + N_{xy}\frac{\partial \Delta w}{\partial x} + \\ &\Delta N_{xy}\frac{\partial w}{\partial x} + \Delta N_{xy}\frac{\partial \Delta w}{\partial x} + \frac{\partial \Delta M_{yy}}{\partial y} + 2\frac{\partial \Delta M_{xy}}{\partial x} + \Delta Q^i_{yy} = 0 \qquad \text{or} \qquad \Delta w = \Delta \bar{w} \end{aligned} \tag{6}$$

where $\bar{u}$, $\bar{v}$ and $\bar{w}$ are the external deformations at the edges; and $i = 0$ at $y = 0$ and $i = b$ at $y = b$.

Constitutive relations

As mentioned before, the concrete is considered as linear viscoelastic, and the steel reinforcement is modelled as elastic. A rheological model which is based on the generalized Maxwell chain is used to formulate the long-term constitutive relations of concrete (Bažant and Wu 1974). The relaxation moduli can be approximated as follows:

$$R_{xx}(t,t') = \frac{E_c}{(1-\nu)\left[1+\varphi(t,t')\right]}; \qquad R_{yy}(t,t') = \frac{E_c}{(1-\nu)\left[1+\varphi(t,t')\right]}; \qquad R_{xy}(t,t') = \frac{G_c}{1+\varphi(t,t')} \tag{7}$$

where $R_{xx}(t,t')$, $R_{yy}(t,t')$ and $R_{xy}(t,t')$ are the relaxation moduli in x and y directions and xy plane; $\varphi(t,t')$ is the creep coefficient of the concrete at time t for a load applied at time t' ; E_c and G_c are the elastic and shear moduli of concrete and ν is the Poisson's ratio, which is assumed to be time-independent (Bazant 1988). Thus, due to the lack of experimental data regarding the creep behavior of concrete in shear, the latter is assumed to be similar to the creep behavior under normal stresses. The relaxation moduli can be expanded into Dirichlet series as follows:

$$R_{xx}(t,t') \approx \bar{R}_{xx}(t,t') = \sum_{\mu=1}^{m} E_\mu e^{-(t-t')/\tau_\mu} + E_{m+1} \quad ; \quad R_{yy}(t,t') \approx \bar{R}_{yy}(t,t') = \sum_{\mu=1}^{m} E_\mu e^{-(t-t')/\tau_\mu} + E_{m+1} \tag{8}$$

$$R_{xy}(t,t') \approx \bar{R}_{xy}(t,t') = \sum_{\mu=1}^{m} G_\mu e^{-(t-t')/\tau_\mu} + G_{m+1} \tag{9}$$

where $\bar{R}_{xx}$, $\bar{R}_{yy}$ and $\bar{R}_{xy}$ are the approximated relaxation moduli; E_μ and G_μ are the moduli of the μth spring in the Maxwell chain for the modelling in the normal and shear directions; m is the number of units; τ_μ is the relaxation time of the μth unit. Note that in this study, m and τ_μ are assumed to be identical in the normal and shear directions for simplicity. The incremental constitutive relations of plane stress state can be formulated as follows based on numerical time integration

$$\Delta\sigma_{xx}(t_r) = \frac{E''(t_r)}{1-\nu^2}\left[\Delta\varepsilon_{xx}(t_r) - \Delta\varepsilon''_{xx}(t_r) + \nu\left(\Delta\varepsilon_{yy}(t_r) - \Delta\varepsilon''_{yy}(t_r)\right)\right] \tag{10}$$

$$\Delta\sigma_{yy}(t_r) = \frac{E''(t_r)}{1-\nu^2}\left[\Delta\varepsilon_{yy}(t_r) - \Delta\varepsilon''_{yy}(t_r) + \nu\left(\Delta\varepsilon_{xx}(t_r) - \Delta\varepsilon''_{xx}(t_r)\right)\right]; \quad \Delta\sigma_{xy}(t_r) = G''(t_r)\left(\Delta\gamma_{xy}(t_r) - \Delta\gamma''_{xy}(t_r)\right) \tag{11}$$

where $E''_c(t_r)$ and $G''(t_r)$ are the pseudo normal and shear moduli, and $\Delta\varepsilon''_{xx}(t_r)$, $\Delta\varepsilon''_{yy}(t_r)$ and $\Delta\gamma''_{xy}(t_r)$ are the incremental prescribed normal strains in x and y directions and shear strain in the xy plane that includes the effect of creep. These are given by

$$E''(t_r) = \sum_{\mu=1}^{m}\left(1-e^{-\Delta t_r/\tau_\mu}\right)\frac{\tau_\mu}{\Delta t_r}E_\mu + E_{m+1}; \quad G''(t_r) = \sum_{\mu=1}^{m}\left(1-e^{-\Delta t_r/\tau_\mu}\right)\frac{\tau_\mu}{\Delta t_r}G_\mu + G_{m+1} \tag{12}$$

$$\Delta\varepsilon''_{xx}(t_r) = \frac{1}{E''(t_r)}\sum_{\mu=1}^{m}\left(1-e^{-\Delta t_r/\tau_\mu}\right)\left[\sigma_\mu^{xx}(t_{r-1}) - \nu\sigma_\mu^{yy}(t_{r-1})\right] \tag{13}$$

$$\Delta\varepsilon''_{yy}(t_r) = \frac{1}{E''(t_r)}\sum_{\mu=1}^{m}\left(1-e^{-\Delta t_r/\tau_\mu}\right)\left[\sigma_\mu^{yy}(t_{r-1}) - \nu\sigma_\mu^{xx}(t_{r-1})\right]; \quad \Delta\gamma''_{xy} = \frac{1}{G''(t_r)}\sum_{\mu=1}^{m}\left(1-e^{-\Delta t_r/\tau_\mu}\right)\sigma_\mu^{xy}(t_{r-1}) \tag{14}$$

$$\sigma_\mu^{xx}(t_r) = e^{-\Delta t_r/\tau_\mu}\sigma_\mu^{xx}(t_{r-1}) + \frac{E_\mu}{1-\nu^2}\left[\Delta\varepsilon_{xx}(t_r) + \nu\Delta\varepsilon_{yy}(t_r)\right]\left(1-e^{-\Delta t_r/\tau_\mu}\right)\frac{\tau_\mu}{\Delta t_r} \tag{15}$$

$$\sigma_\mu^{yy}(t_r) = e^{-\Delta t_r/\tau_\mu}\sigma_\mu^{yy}(t_{r-1}) + \frac{E_\mu}{1-\nu^2}\left[\Delta\varepsilon_{yy}(t_r) + \nu\Delta\varepsilon_{xx}(t_r)\right]\left(1-e^{-\Delta t_r/\tau_\mu}\right)\frac{\tau_\mu}{\Delta t_r} \tag{16}$$

$$\sigma_\mu^{xy}(t_r) = e^{-\Delta t_r/\tau_\mu}\sigma_\mu^{xy}(t_{r-1}) + G_\mu\Delta\gamma_{xy}(t_r)\left(1-e^{-\Delta t_r/\tau_\mu}\right)\frac{\tau_\mu}{\Delta t_r} \tag{17}$$

where σ_μ^{xx}, σ_μ^{yy} and σ_μ^{xy} are the stresses in the μth Maxwell unit. $G''(t_r)$ and G_μ are given by $G''(t_r) = E''(t_r)/[2(1+\nu)]$ and $G_\mu = E_\mu/[2(1+\nu)]$.

The constitutive relations at the cross-section level of the panel are determined using the classical definition of stress resultants and using the constitutive relations (Eqs 10 and 11) and the kinematic relations (Eq. 1) as follows:

$$\Delta N_{xx}(t_r) = C''\left[\frac{\partial\Delta u}{\partial x} + \frac{1}{2}\left(\frac{\partial\Delta w}{\partial x}\right)^2 + \frac{\partial w(t_{r-1})}{\partial x}\frac{\partial\Delta w}{\partial x} + \nu\left(\frac{\partial\Delta v}{\partial y} + \frac{1}{2}\left(\frac{\partial\Delta w}{\partial y}\right)^2 + \frac{\partial w(t_{r-1})}{\partial y}\frac{\partial\Delta w}{\partial y}\right)\right] - \Delta\bar{N}_{xx}(t_r) \tag{18}$$

$$\Delta N_{yy}(t_r) = C''\left[\frac{\partial\Delta v}{\partial y} + \frac{1}{2}\left(\frac{\partial\Delta w}{\partial y}\right)^2 + \frac{\partial w(t_{r-1})}{\partial y}\frac{\partial\Delta w}{\partial y} + \nu\left(\frac{\partial\Delta u}{\partial x} + \frac{1}{2}\left(\frac{\partial\Delta w}{\partial x}\right)^2 + \frac{\partial w(t_{r-1})}{\partial x}\frac{\partial\Delta w}{\partial x}\right)\right] - \Delta\bar{N}_{yy}(t_r) \tag{19}$$

$$\Delta N_{xy}(t_r) = \frac{1-\nu}{2}C''\left[\frac{\partial\Delta u}{\partial y} + \frac{\partial\Delta v}{\partial x} + \frac{\partial w(t_{r-1})}{\partial x}\frac{\partial\Delta w}{\partial y} + \frac{\partial w(t_{r-1})}{\partial y}\frac{\partial\Delta w}{\partial x} + \frac{\partial\Delta w}{\partial x}\frac{\partial\Delta w}{\partial y}\right] - \Delta\bar{N}_{xy}(t_r) \tag{20}$$

$$\Delta M_{xx}(t_r) = -D''\left(\frac{\partial^2\Delta w}{\partial x^2} + \nu\frac{\partial^2\Delta w}{\partial y^2}\right) - \Delta\bar{M}_{xx}(t_r); \qquad \Delta M_{yy}(t_r) = -D''\left(\frac{\partial^2\Delta w}{\partial y^2} + \nu\frac{\partial^2\Delta w}{\partial x^2}\right) - \Delta\bar{M}_{yy}(t_r) \tag{21}$$

$$\Delta M_{xy}(t_r) = -(1-\nu)D''\frac{\partial^2\Delta w}{\partial x\partial y} - \Delta\bar{M}_{xy}(t_r) \tag{22}$$

where C'' and D'' are axial and flexural viscoelastic rigidities of the two-way panel; $\Delta\bar{N}_{xx}(t_r)$, $\Delta\bar{N}_{yy}(t_r)$ are the incremental effective axial forces in the x and y directions and $\Delta\bar{N}_{xy}(t_r)$ is the incremental effective shear force in

the *xy* plane; $\Delta\bar{M}_{xx}(t_r)$ and $\Delta\bar{M}_{yy}(t_r)$ are the incremental effective bending moments along *x* and *y* axis and $\Delta\bar{M}_{xy}(t_r)$ is the incremental effective torsional bending moment. Note that the forces and bending moments are defined as the distributions of these quantities per unit width. The viscoelastic rigidities, which account for the internal reinforcement, are given by

$$C'' = \frac{E''}{1-\nu^2}\left[h + (n-1)A_s / b + (n-1)A_s' / b\right]; \quad D'' = \frac{E''}{1-\nu^2}\left[\frac{h^3}{12} + (n-1)A_s z_s^2 / b + (n-1)A_s' z_s'^2 / b\right] \tag{23}$$

where *h* is the thickness of the panel; $n = E_s / E''$, E_s is elastic modulus of steel reinforcement; A_s and A_s' are the areas of the steel reinforcements at the inner and outer faces of the panel; z_s and z_s' are the locations of the corresponding reinforcements measured from the mid-thickness of the panel. For simplicity, A_s and A_s' are taken as the minimum reinforcement ratios between *x* and *y* directions. The effective forces and bending moments are given as

$$\Delta\bar{N}_{xx}(t_r) = \sum_{\mu=1}^{m}\left(1-e^{-\Delta t_r/\tau_\mu}\right)N_\mu^{xx}(t_{r-1}) + \int_{-\frac{h}{2}}^{\frac{h}{2}} \frac{E''(t_r)}{1-\nu}\Delta\varepsilon_{sh}\,\mathrm{d}z; \quad \Delta\bar{N}_{yy}(t_r) = \sum_{\mu=1}^{m}\left(1-e^{-\Delta t_r/\tau_\mu}\right)N_\mu^{yy}(t_{r-1}) + \int_{-\frac{h}{2}}^{\frac{h}{2}} \frac{E''(t_r)}{1-\nu}\Delta\varepsilon_{sh}\,\mathrm{d}z \tag{24}$$

$$\Delta\bar{N}_{xy}(t_r) = \sum_{\mu=1}^{m}\left(1-e^{-\Delta t_r/\tau_\mu}\right)N_\mu^{xy}(t_{r-1}) + \int_{-\frac{h}{2}}^{\frac{h}{2}} \frac{E''(t_r)}{2(1+\nu)}\Delta\varepsilon_{sh}\,\mathrm{d}z; \quad \Delta\bar{M}_{xx}(t_r) = \sum_{\mu=1}^{m}\left(1-e^{-\Delta t_r/\tau_\mu}\right)M_\mu^{xx}(t_{r-1}) + \int_{-\frac{h}{2}}^{\frac{h}{2}} \frac{E''(t_r)z}{1-\nu}\Delta\varepsilon_{sh}\,\mathrm{d}z \tag{25}$$

$$\Delta\bar{M}_{yy}(t_r) = \sum_{\mu=1}^{m}\left(1-e^{-\Delta t_r/\tau_\mu}\right)M_\mu^{yy}(t_{r-1}) + \int_{-\frac{h}{2}}^{\frac{h}{2}} \frac{E''(t_r)z}{1-\nu}\Delta\varepsilon_{sh}\,\mathrm{d}z; \quad \Delta\bar{M}_{xy}(t_r) = \sum_{\mu=1}^{m}\left(1-e^{-\Delta t_r/\tau_\mu}\right)M_\mu^{xy}(t_{r-1}) + \int_{-\frac{h}{2}}^{\frac{h}{2}} \frac{E''(t_r)z}{2(1+\nu)}\Delta\varepsilon_{sh}\,\mathrm{d}z \tag{26}$$

Governing Equations

The incremental governing equations are formulated by substitution of the stress resultants (Eqs 18-22) into the equilibrium equations (Eqs 3 and 4), noting that terms of higher product of the incremental displacements and forces are neglected due to the use of sufficiently small time increments. The incremental governing equations are partial differential equations in terms of the unknown displacements:

$$\psi_p\left(\Delta u,\ \Delta v,\ \Delta w\right) = 0 \qquad \left(p = 1,\ 2,\ 3\right) \tag{27}$$

where ψ_p consists of differential operators. For brevity, the explicit form of these equations is not presented here. The equations and the boundary conditions (Eqs 5 and 6) are reduced to a set of ordinary differential equations by a separation of variables and expansion into the truncated Fourier series (Hong and Teng 2002; Hamed et al., 2010).

$$\left\{\Delta u(x,y),\ \Delta v(x,y),\ \Delta w(x,y)\right\} = \sum_{m=1}^{2F}\left\{\Delta u_m(x),\ \Delta v_m(x),\ \Delta w_m(x)\right\}g_m(y) \tag{28}$$

where F = (F_u, F_v, or F_w) is the number of terms in the relevant Fourier series. The initial state or previous accumulated displacements and the external loads along the panel and at the boundaries take the following form

$$\left\{u(x,y),\ v(x,y),\ w(x,y)\right\} = \sum_{m=1}^{2F}\left\{u_m(x),\ v_m(x),\ w_m(x)\right\}g_m(y) \tag{29}$$

$$\begin{Bmatrix} Q_{xx}^0(x,y),\ Q_{xx}^a(x,y), N_{xx}^0(x,y), \\ N_{xx}^a(x,y), M_{xx}^0(x,y),\ M_{xx}^a(x,y) \end{Bmatrix} = \sum_{m=1}^{2F}\begin{Bmatrix} Q_{xxm}^0(x),\ Q_{xxm}^a(x), N_{xxm}^0(x), \\ N_{xxm}^a(x), M_{xxm}^0(x),\ M_{xxm}^a(x) \end{Bmatrix} g_m(y)$$

$$\begin{Bmatrix} Q_{yy}^0(x,y),\ Q_{yy}^b(x,y), N_{yy}^0(x,y), \\ N_{yy}^b(x,y), M_{yy}^0(x,y),\ M_{yy}^b(x,y) \end{Bmatrix} = \sum_{m=1}^{2F}\begin{Bmatrix} Q_{yym}^0(x),\ Q_{yym}^b(x), N_{yym}^0(x), \\ N_{yym}^b(x), M_{yym}^0(x),\ M_{yym}^b(x) \end{Bmatrix} g_m(y) \tag{30}$$

$$q_z(x,y) = \sum_{m=1}^{2F} q_{zm}(x)g_m(y)$$

The functions $g_m(y)$ are

$$g_m(y) = \begin{cases} \sin\left(\dfrac{m\pi}{b}y\right) & m = 1, 2, \ldots, F \\ \cos\left[\dfrac{(m-F)\pi}{b}y\right] & m = F+1, F+2, \ldots, 2F \end{cases} \tag{31}$$

By minimizing the errors due to the truncated Fourier series by the Galerkin procedure with trigonometric weighting functions, the partial differential equations are converted into linear ordinary differential equations in the x direction:

$$\Psi_p^m(x) = \int_0^b \psi_p\left(u,\ v,\ w\right) g_m(y)\mathrm{d}y \qquad \left(p = 1,\ 2,\ 3;\ \ m = 1, 2, ..., 2F\right) \tag{32}$$

The governing equations along with the boundary conditions are solved through the use of the multiple shooting method at each time step (Stoer and Bulirsch 2002). The analysis presented here is also conducted up to a certain time (the critical time) where the deformations of the system exceed a prescribed limit (Hoff 1958; Bažant and Cedolin 1991). A proper time step is selected for a given load level in the way that the difference between the predicted critical times of creep buckling for the selected time-step and one-half of it is of minor significance.

NUMERICAL STUDY

The governing equations derived in Eq. 27 and the solution procedures proposed in Eqs 28-31 are generally applicable for any combinations of loading scenarios and boundary conditions. Here, a square panel that is simply-supported on four edges and subjected to an in-pane eccentric compression load in the x direction only, as shown in Figure 2, is investigated. For this particular case, only the first term of the Fourier series is considered.

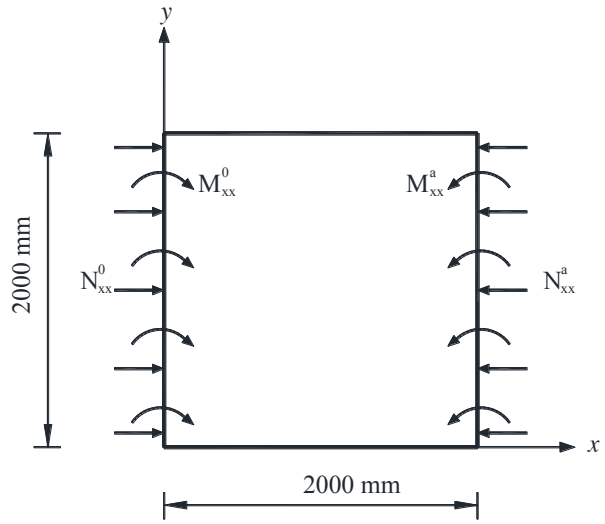

Figure 2 HSC panel used in numerical study: simply-supported on four edges and loaded by uniformly distributed eccentric compression forces in the x direction

The thickness of the panel is 100 mm. There are two layers of steel reinforcement in both orthogonal directions, placed at top and bottom of the specimen. The reinforcement ratios in the x and y directions (ρ_x and ρ_y), where $\rho_x = (A_{sx} + A'_{sx})/bh$ and $\rho_y = (A_{sy} + A'_{sy})/ah$, are both 0.2% and the reinforcement at the top and bottom layers in each direction are equal. The concrete cover is 20 mm and the elastic modulus of the steel is 200 GPa, respectively. The panel is assumed to be loaded at the age of 28 days after casting with $N^0_{xx} = N^a_{xx} = 20.3$ kN/mm. The applied load equals to 60% of the instantaneous classical buckling load (P_{cr} = 33.9 kN/mm), that is determined as follows (Dym and Shame 2013):

$$P_{cr} = \frac{4D''\pi^2}{b^2} = \frac{4\pi^2}{b^2}\frac{E_c}{1-\nu^2}\left[\frac{h^3}{12} + (n-1)A_s z_s^2 / b + (n-1)A'_s z'^2_s / b\right] \tag{33}$$

The load eccentricity is $e = h/6 = 16.7$ mm, which results in edge moments of $M^0_{xx} = M^a_{xx} = 339$ kNm/m (Figure 2). The development with time of the creep coefficient is calculated according to AS3600 (2009) as follows

$$\varphi(t) = \frac{1.45t^{0.8}}{t^{0.8} + 17} \tag{34}$$

The number of Maxwell units (m) used to model the viscoelastic behavior of concrete is taken as five in this example with $\tau_\mu = 5^{\mu-1}$ (days). The spring constants in the Maxwell model obtained by the least squares methods are E_1 = 1684 MPa, E_2 = 7537 MPa, E_3 = 8674 MPa, E_4 = 4050 MPa, E_5 = 1199 MPa, E_6 = 16287 MPa.

The time-dependent variation of the out-of-plane deflection and the bending moments at the center of the panel are shown in Figure 3. The time t is measured from the time of first loading. The deflection is normalized with respect to the thickness of the panel h. It can be seen that the deflection of the panel and hence the bending moments M_{xx} and M_{yy} increase with time as a result of the combined effects of creep and geometric nonlinearity. Similar to the one-way panel, the out-of-plane deflection as well as the bending moments exhibit unlimited asymptotical increase beyond a certain time. The criterion for critical time of buckling failure adopted here is when the normalized out-of-plane deflection (w/h) reaches a given limit (Hoff 1958; Bažant and Cedolin 1991). The limit in this numerical study is taken as 4 and the corresponding time, referred to as the critical time, equals 1400 days in this case. As indicated in Figure 3d, the ratio of M_{xx}/M_{yy} also increases with time, which implies that stress redistribution occurs with time and the influence of the geometric nonlinearity becomes more pronounced in the x direction than in the y direction.

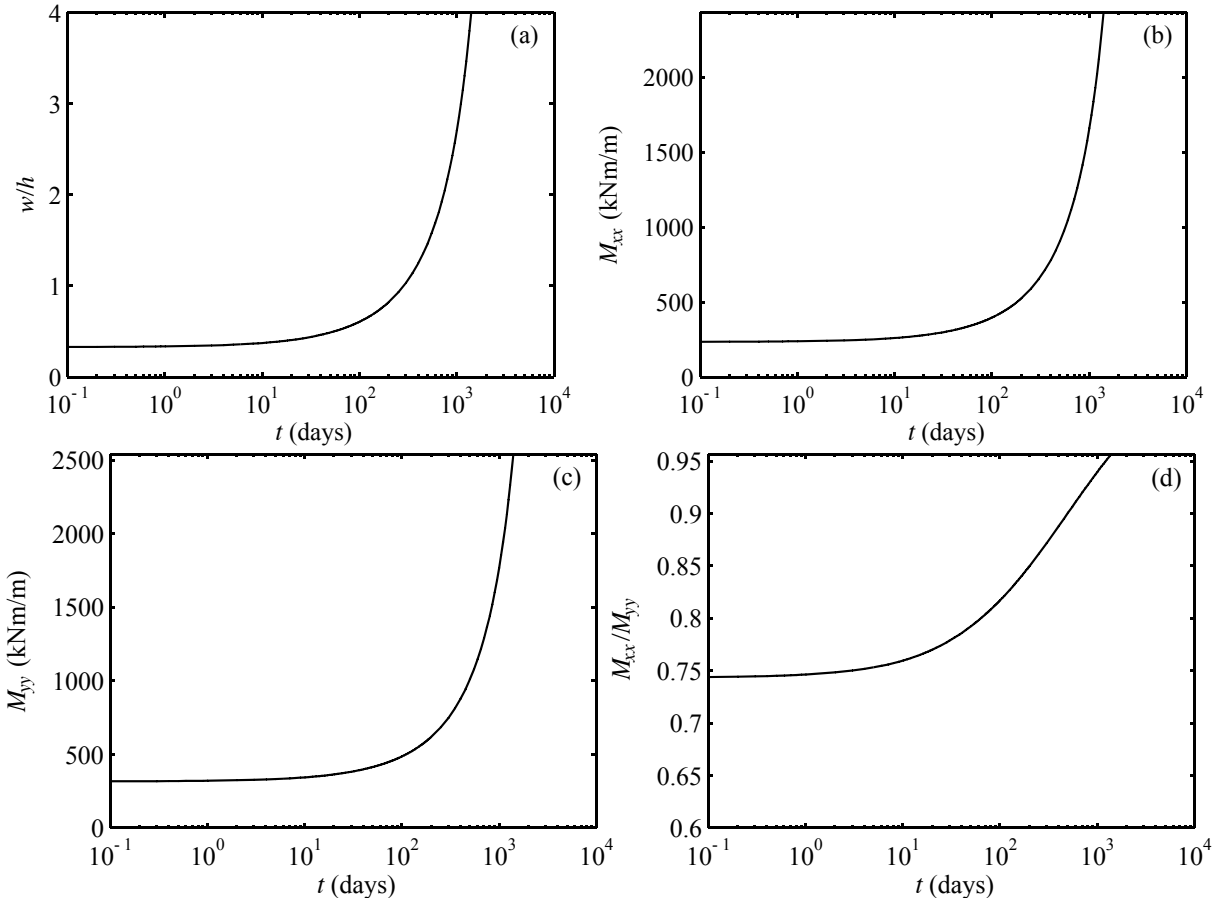

Figure 3 Variation with time of the (a) out-of-plane deflection; (b) bending moment M_{xx}; (c) the bending moment M_{yy}; (d) the ratio of M_{xx}/M_{yy} at the center of the panel

A parametric study is conducted here to examine the effects of key parameters on the time-dependent response of HSC panels. The parameters include the magnitude and eccentricity of the sustained in-plane load (N_{xx}^{0}) and the slenderness ratio defined as a/h. The panel investigated in the numerical example is used as a reference and the reinforcement ratio is constant.

Figure 4 presents the influence of the level of the sustained load on the time-dependent behaviour. It can be seen that the increase of the imposed load level leads to earlier occurrence of buckling (shorter critical time). It can also be observed that the panel studied here is stable in the long run under a load level that is lower than 50% of the elastic buckling load P_{cr}, as the increase in the out-of-plane deflection becomes insignificant after a certain time, which can be critical for the design of HSC panels. The minimum load level to cause creep buckling for the examined panel is 51% of its elastic buckling load. This result is in accordance with that obtained using the simplified Effective Modulus Method (EMM), where E_c in Eq. 33 is replaced with $E_c / \left[1+\varphi(t,t')\right]$.

Nevertheless, if cracking is taken into account or biaxial loading scenarios are considered, the simplified effective modulus method might lead to inaccurate results.

Figure 5 reveals the change of the out-of-plane deflection at the centre of the square panel with time under the in-plane compression load with different eccentricities. The load is equal to 52% of the elastic buckling load. As seen in the figure, the time-dependent behaviour is very sensitive to the eccentricity. Thus, it is essential in the design to consider different load scenarios as small inaccuracy in estimating the actual load eccentricity may result in catastrophic buckling failure in the long term.

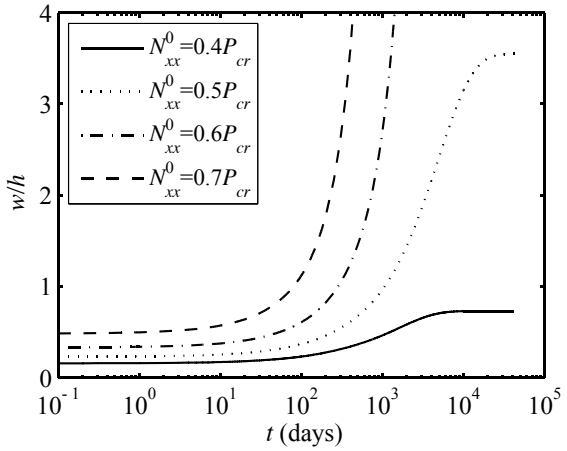

Figure 4 Influence of load level ($e = h/6$, $[\rho_x, \rho_y] = 0.2\%$, $a \times b \times h = 2000 \times 2000 \times 100$ mm)

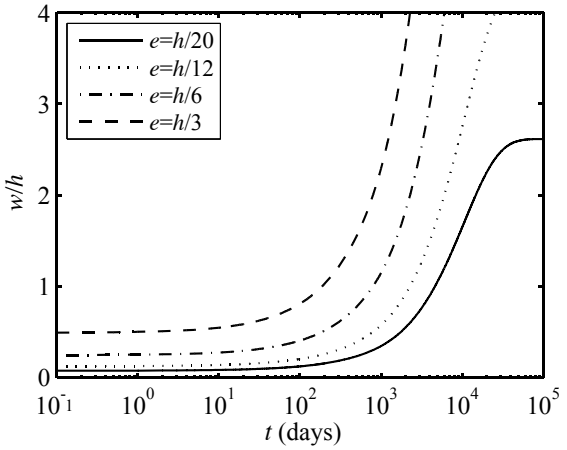

Figure 5 Influence of load eccentricity ($N^0_{xx} = 0.52P_{cr}$, $[\rho_x, \rho_y] = 0.2\%$, $a \times b \times h = 2000 \times 2000 \times 100$ mm)

The normalized deflection at the center of the panels with various thicknesses is plotted against time in Figure 6 for investigating the effect of slenderness of the panel. The load level, the eccentricity as well as the reinforcement ratios in both orthogonal directions are $0.6P_{cr}$, $h/6$, and 0.2%, respectively, where P_{cr} is the elastic buckling load corresponding to the panel with 100 mm thickness in order to keep the load unchanged for the three different cases. The slenderness ratio is defined as a/h. Three different thicknesses 90 mm, 100 mm and 120 mm are investigated, which yield slenderness ratios of 22.2, 20 and 16.7, respectively. It can be seen that under the same magnitude of sustained load, the panels that are 90 mm and 100 mm thick are unstable whereas the panel with 120 mm thickness exhibits stable behavior. For the unstable panels, the critical time increases with increasing the thickness. Therefore, in practical design and use of two-way panels, the creep buckling failure can be potentially prevented by slightly increasing the thickness of the panel.

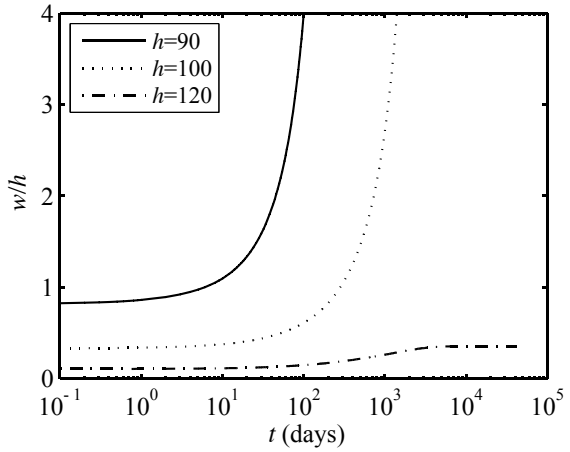

Figure 6 Influences of slenderness ($N_{xx}^{0} = 0.6P_{cr}$, $e = h/6$, $[\rho_x, \rho_y] = 0.2\%$, $a \times b = 2000 \times 2000$ mm)

CONCLUSIONS

A theoretical model is developed in this paper for the time-dependent analysis of two-way HSC panels. Creep of the concrete is accounted for through a rheological viscoelastic model. The model considers the geometric nonlinearity and describes the variation of the internal stresses with time through a step-by-step time analysis. It has been shown in the numerical study that the increase of out-of-plane deflection and the internal bending moments may lead to creep buckling failures under axial sustained loads that are as low as 50% of the instantaneous classical buckling load. The parametric study reveals that the creep buckling response of HSC panels is very sensitive to key parameters including the load level and eccentricity as well as the slenderness ratio.

ACKNOWLEGEMENTS

The work reported in this paper was supported by the Australian Research Council through a Discovery Project (DP 120102762).

REFERENCES

Aghayere, A. O., and Macgregor, J. G. (1990a). "Tests of reinforced concrete plates under combined in-plane and transverse loads." *ACI Structural Journal*, 87(6), 615-622.

Aghayere, A. O., and MacGregor, J. G. (1990b). "Analysis of concrete plates under combined in-plane and transverse loads." *ACI Structural Journal*, 87(5), 539-547.

AS3600 (2009). "Concrete structures." *AS3600-2009*, Standards Association of Australia, Sydney, Australia

Attard, M. M., Minh, N. G., and Foster, S. J. (1996). "Finite element analysis of out-of-plane buckling of reinforced concrete walls." *Computers and Structures*, 61(6), 1037-1042.

Bazant, Z. P. (1988). *Mathematical modelling of creep and shrinkage of concrete*, John Wiley and Sons, Chichester.

Bažant, Z. P., and Wu, S. T. (1974). "Rate-type creep law of aging concrete based on maxwell chain." *Materials and Structures*, 7(1), 45-60.

Bažant, Z. P., and Cedolin, L. (1991). *Stability of structures: Elastic, inelastic, fracture and damage theories*, Oxford University Press, New York.

Dym, C. L., and Shame, I. H. (2013). *Solid mechanics a variational approach* Springer Science+Business Media New York, Heidelberg, Dordrecht, London.

Ghoneim, M. G., and MacGregor, J. G. (1994a). "Tests of reinforced concrete plates under combined inplane and lateral loads." *ACI Structural Journal*, 91(1), 19-30.

Ghoneim, M. G., and MacGregor, J. G. (1994b). "Prediction of the ultimate strength of reinforced concrete plates under combined inplane and lateral loads." *ACI Structural Journal*, 91(6), 688-696.

Hamed, E., Bradford, M. A., and Gilbert, R. I. (2010). "Creep buckling of imperfect thin-walled shallow concrete domes." *Journal of Mechanics of Materials and Structures*, 5(1), 107-128.

Hoff, N. J. (1958). "A survey of the theories of creep buckling." *Proc.,3rd US National Congress of Applied Mechanics*, American Society of Mechanical Engineers, New York, United States, 29-49.

Hong, T., and Teng, J. G. (2002). "Non-linear analysis of shells of revolution under arbitrary loads." *Computers and Structures*, 80(18-19), 1547-1568.

Huang, Y., and Hamed, E. (2013). "Buckling of one-way high-strength concrete panels: Creep and shrinkage effects." *Journal of Engineering Mechanics*, 139(12), 1856-1867.
Huang, Y. (2015). "Nonlinear long-term behaviour of high-strength concrete wall panels." PhD Dissertation, The University of New South Wales, Sydney.
Massicotte, B., MacGregor, J. G., and Elwi, A. E. (1990). "Behavior of concrete panels subjected to axial and lateral loads." *Journal of structural engineering New York, N.Y.*, 116(9), 2324-2343.
Saheb, S. M., and Desayi, P. (1990). "Ultimate strength of r.C. Wall panels in two-way in-plane action." *Journal of Structural Engineering*, 116(5), 1384-1402.
Sanjayan, J. G., and Maheswaran, T. (1999). "Load capacity of slender high-strength concrete walls with side supports." *ACI Structural Journal*, 96(4), 571-577.
Stoer, J., and Bulirsch, R. (2002). *Introduction to numerical analysis*, Springer-Verlag, New York.
Swartz, S. E., Rosebraugh, V. H., and Berman, M. A. (1974). "Buckling test on rectangular concrete panels." *ACI Journal*, 71(5), 33-39.
Swartz, S. E., and Rosebraugh, V. H. (1974). "Buckling of reinforced concrete plates." *ASCE J Struct Div*, 100(ST1), 195-208.